Journal of Manufacturing Systems 36 (2015) 231–243

Contents lists available at ScienceDirect

Journal of Manufacturing Systems

journal homepage: www.elsevier.com/locate/jmansys

Technical paper

Optimization of layered manufacturing process for reducing form errors with minimal support structures

Ratnadeep Paul[1], Sam Anand*

Center for Global Design and Manufacturing, Department of Mechanical and Materials Engineering, University of Cincinnati, 598 Rhodes Hall, PO Box 210072, Cincinnati, OH 45221-0072, United States

ARTICLE INFO

Article history:
Received 20 April 2012
Received in revised form 30 May 2014
Accepted 26 June 2014
Available online 23 July 2014

Keywords:
Additive Manufacturing
Layered manufacturing
Form errors
Support structures
Voxels
Multi-objective optimization

ABSTRACT

Layered manufacturing (LM) has evolved from the rapid prototyping (RP) method to a mainstream process for manufacturing high precision parts for aerospace, automotive and medical industries. LM inherits from RP several advantages including the ability to produce complex shapes, low cost and elimination of special tooling, as well as disadvantages of poor surface finish, poor dimensional accuracy, high build time and high waste. As LM is increasingly being accepted as a traditional manufacturing process, it has to consistently manufacture parts with minimal errors while keeping the material utilization to a minimum. This paper analyzes the effect of part orientation on two types of form errors, namely, cylindricity and flatness errors. An algorithm to calculate the optimal orientation for minimizing flatness and cylindricity errors is developed and tested with the help of two test cases. However, an optimal orientation for minimum form errors may result in a greater utilization of support structures which increases the material consumption in LM processes and therefore should be avoided. A voxel-based approach for calculating support structures has been developed in this paper which is then applied to minimize the volume of support structures while minimizing the cylindricity and flatness errors of the part features. This combined optimization is applied on two test parts and the results are provided.
© 2014 The Society of Manufacturing Engineers. Published by Elsevier Ltd. All rights reserved.

1. Introduction

Layered manufacturing (LM) has evolved as the next logical development of the rapid prototyping (RP) paradigm to manufacture complex service parts using a slicing approach. LM processes share the same process parameters with RP, namely layer thickness, part orientation, 2D toolpath and support structures [1]. Part orientation refers to the orientation of the part in which the slices are created while layer thickness refers to the resolution of the slices that are generated. Support structures are used to prop up internal cavities and overhanging features of a part. 2D toolpath refers to the path followed by the tool while creating the individual slices. These process parameters have a considerable effect on the dimensional accuracy of the parts manufactured in LM. In addition to part accuracy, support structures also have a direct impact on the material utilization in the process. As LM is becoming more and more popular, it faces a key challenge to consistently create parts with high degree of accuracy while reducing material expenditure. In general, higher part accuracy in LM can be accomplished by different methods such as adaptive and direct slicing [2–6], using optimal part orientations [7–12] and machining the part during and after build [13]. One of the methods by which the material and energy expenditure in LM processes can be minimized is to reduce the amount of support structures used in the process. Support structures are not part of the final product and are removed at the end of the process by water cleaning or by dissolving in solvents and thus contribute to additional material usage in the process.

LM researchers have traditionally sought to define part accuracy as volumetric and chordal errors. There have been various published studies correlating LM process parameters with the volumetric [9,10] and chordal errors [14–17] in a part manufactured in LM. However, the correlation between process parameters and Geometric Dimensioning and Tolerancing (GD&T) form errors in parts manufactured by LM has not been investigated in detail and only a few papers have been published in this area [18,19]. However, all these papers applied statistical techniques for evaluating the form errors and did not develop the analysis from first principles. To date, only two papers have been published which have developed a mathematical framework for evaluating form errors in LM parts. Paul and Anand [7] studied the effect of part orientation on the cylindricity error of parts with single and multiple

* Corresponding author. Tel.: +1 513 556 5596; fax: +1 513 556 3390.
E-mail addresses: paulrp@ucmail.uc.edu (R. Paul), sam.anand@uc.edu (S. Anand).
[1] Tel.: +1 513 556 5774.

http://dx.doi.org/10.1016/j.jmsy.2014.06.014
0278-6125/© 2014 The Society of Manufacturing Engineers. Published by Elsevier Ltd. All rights reserved.

cylindrical features while Arni and Gupta [12] analyzed the effect of build orientation on flatness errors in LM parts. Furthermore, these two papers only considered each form error individually and did not look into the effect of part orientation on combined form errors. In addition to the study of form errors in LM processes and their correlation to process parameters, the inter-dependence of support structures and form errors is also another field which has not received much attention from LM researchers. The current paper, therefore, presents a detailed mathematical analysis of the relationship between the form errors in part features, support structure volume and the build orientation for LM processes. The overall objective of this work is to develop a unified approach for minimizing form errors on precision parts manufactured in LM processes while simultaneously striving for the minimal consumption of raw materials in the form of support structures.

As a first step, a multi factor optimization approach has been developed in this paper to minimize two major form tolerances-cylindricity and flatness errors-as functions of part orientation. The feasible regions of the part build orientation for cylindricity and flatness errors are mapped from a 3D Euclidean space on to a 1D line using trigonometric functions, thereby reducing the order and complexity of the problem. Next, this 1D line parameter space is employed to generate a combined error function which correlates the flatness and cylindricity errors on the critical features to the part build orientation. The error function is then used as the objective function in an optimization model to calculate the optimal part orientation for minimum form errors. This model is tested on two sample parts with multiple planar and cylindrical features and the results are provided.

In the second step, the amount of raw material used in the LM process is minimized by reducing the volume of support structures. A voxel-based algorithm for calculating the support structures in any generic LM process is introduced. Voxels (volumetric pixels) are 3D array of cubes which can be used to represent any CAD model. Voxels are widely used for visualization and representation of spatial data in medical imaging, computer gaming technologies, remote sensing, etc. [20–23]. The stereolithography (STL) file of the part is converted to a voxel representation and the voxels are used to calculate the amount of support structures for any particular orientation. The algorithm is tested by calculating the support structures for two simple parts. The methodology is then applied to find the optimal part orientation that corresponds to the minimum support structure volume.

Finally, the form error function and the support structure volume function are combined into a single aggregate objective function (AOF) to calculate the part build orientation which will simultaneously minimize cylindricity and flatness form errors and the volume of support structures. Since the form error function is in the range of 0–1, the support structure volume is also normalized to that range. This normalized AOF is applied on two test parts to find the optimal orientation and the results are provided. This combined approach will provide designers and engineers a methodology for selecting the best part orientation for manufacturing high precision parts with minimal form errors and minimal support structures.

The rest of the paper is divided into six sections. Section 2 provides a brief description of the research conducted in the fields of LM processes, geometric tolerances and calculation of support structures. Section 3 describes the algorithm for calculating the optimal orientation of a part which will lead to minimum cylindricity and flatness errors on the manufactured part in an LM process. Section 4 describes a method to compute the volume of support structures using a voxel representation while Section 5 describes the algorithm for computing the part build direction for achieving the minimum support structure volume. Section 6 presents a combined optimization model which minimizes the flatness and cylindricity errors together with the support structure volume in an LM process. Finally, Section 7 provides the conclusions and future scope of this research.

2. Literature review

In LM processes, slice thickness and part orientation have a direct impact on the accuracy of the manufactured part. Due to the increasing popularity of LM, researchers have recently started focusing on the effect of these parameters on the form errors in the final manufactured part. Another LM process parameter, support structures, is used to prop internal cavities and overhanging and disconnected features during the part build. Support structures also have a considerable effect on the part strength and accuracy. The calculation of support structure is not straightforward and several researchers have developed different methods to determine the amount of support structures required during the part build in RP/LM [24–28]. This section describes the research conducted in these areas and is divided into two main parts: (1) Form errors in RP/LM processes and (2) Support structures in RP/LM.

2.1. Form errors in RP/LM processes

As LM is slowly evolving into a mainstream manufacturing process, the process capabilities of LM to produce highly accurate parts are being investigated by researchers. Arni and Gupta [12] studied the effect of orientation on the flatness error induced in a planar feature in an LM part. They calculated the flatness error for a particular orientation and using Gaussian spheres, determined the best candidate orientations to achieve the required flatness tolerances in a part. Hanumaiah and Ravi [18] conducted an experimental study on the straightness, flatness and circularity errors of parts built by the SLA and direct metal laser sintering (DMLS) processes. They generated eight parts and using an adaptive sampling procedure, calculated the different errors using the least-squares method. Their study calculated the errors for the various parts but did not correlate them with the process parameters. Ollison and Berisso [19] performed an experimental study on cylindricity error for parts built by the 3D printing process. They used an ANOVA model for their study and according to their results the cylindricity error is minimum at a build orientation of 0 degrees, followed by 45 and 90 degrees. Although the paper correlated the cylindricity of a part to the build orientation, the model used in the paper was simplified and considered only three build directions. Recently, Paul and Anand [7] performed a detailed analysis on the effect of orientation on cylindricity error for single and multiple cylindrical features in a part. They calculated the cylindricity error by: (a) performing geometric analysis and (b) modeling the process and simulating the cylinder surface from CAD and STL models. Lynn and Rosen [29] studied the effect of process parameters on six tolerances: positional, flatness, parallelism, perpendicularity, concentricity and circularity on a variety of geometries using the response surface methodology (RSM). They used wait time, slice thickness, overcure and sweep period as their input variables in their design of experiment study and used a second order response surface to correlate the part errors with the inputs. Masood and Rattanawong [9,10] calculated the volumetric error of the final part manufactured in LM using a geometric model and correlated this error to the build orientation. Liu et al. [30] studied the cusp height error in an RP part using second order surface approximations and developed a mathematical model to calculate this error. To date, only two papers [7,12] have developed mathematical models for correlating LM parameters with form errors.

2.2. Support structures in RP/LM

Support structures are extra materials added to the part during the part build to support holes and disjointed features [1]. Support structures are removed from the final part during post processing and therefore, the process parameters should be chosen such that the amount of support structures is minimized. The importance of support structures in LM processes makes their study imperative and some of the published research has been reported in this section.

Majhi et al. [28] developed a 2D algorithm for finding the trapped area of material in an LM processes. They found edges pointing downwards and calculated the area of the trapped support structures from these edges. In an extension of this paper, Majhi et al. [27] used a computational geometry approach to solve the problem of support structure calculation in 3D space. They developed an algorithm to calculate the minimum volume support structures for convex polyhedrons in O (n^2) time, where n is the number of faces. Allen and Dutta [24] computed the amount of support structures required in an LM processes using a facet normal approach and calculated the possible orientation candidates for minimum support structures using a convex hull methodology. In another paper, Allen and Dutta [26] developed an alternative for support structures in RP for manufacturing thin-walled parts. They locally increased the wall thickness for overhanging features which would provide supports for those features. Alexander and Dutta [31] extended this method to thin-walled parts with open contours. They also calculated the orientation for minimizing the localized wall thicknesses of critical features. Yang et al. [32] proposed a new multi-orientation deposition technique to minimize the support structures using the successive layer area difference as the determining parameter. All these papers take into account only convex parts or approximate non-convex parts using the convex hull for calculating the support structures. The current paper presents a novel 3-D grid approach for calculating the location and volume of support structures for convex as well as non-convex parts.

The rest of the paper describes the methodology for calculating the optimal orientation which will result in the minimization of form errors in the critical features of an LM part. Two error functions have been developed which correlate the cylindricity and flatness errors to part orientation and these error functions have been applied to develop a combined optimization model.

3. Optimal build direction for multiple features

The form errors that have been studied in this paper are flatness and cylindricity errors since these are the most common callouts specified in part designs. In LM, the part build orientation along with other process parameters should be chosen such that the flatness and cylindricity tolerances specified on each part feature are satisfied. This section describes an algorithm that calculates the optimal part orientation which leads to the combined minimization of cylindricity and flatness errors in the part manufactured in LM.

Paul and Anand [7] analyzed the relation between cylindricity error and part orientation in an LM orientation by three methods: (a) A simple geometric model, (b) Simulating the virtual manufactured surface of a CAD cylinder and (c) Simulating the virtual manufactured surface of an STL file. According to their calculations, the major geometric source of cylindricity error is the staircase effect and the cylindricity error (ε_{cyl}) obtained by the first two methods have a similar sinusoidal relation with the part orientation which is defined as the angle (γ) between the cylinder axis ($\overrightarrow{ca}$) and build vector ($\overrightarrow{bv}$). The cylindricity error obtained from the STL file also has a sinusoidal relation with the orientation but is offset by a small amount from the analytic geometric model and the CAD cylinder, as shown in Fig. 1. The cylindricity error for the STL file is more than the CAD model because the STL file is an approximation of the cylinder while the CAD model is the true representation. Considering the STL curve in Fig. 1, if a tolerance callout, ε_{sp_cyl}, is specified for any cylinder, then there exists two critical values of the build orientation γ_{cr1} and γ_{cr2}, such that if the part build orientation lies within these critical values, the cylindricity error on the part will be within the specified tolerance. These critical regions for cylindricity error are shown in Fig. 2.

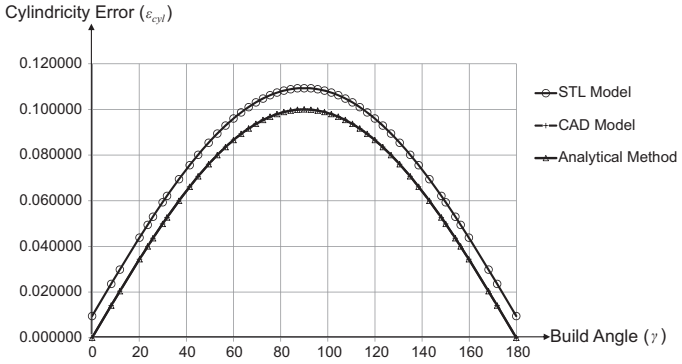

Fig. 1. Cylindricity error vs cylinder orientation in LM [7].

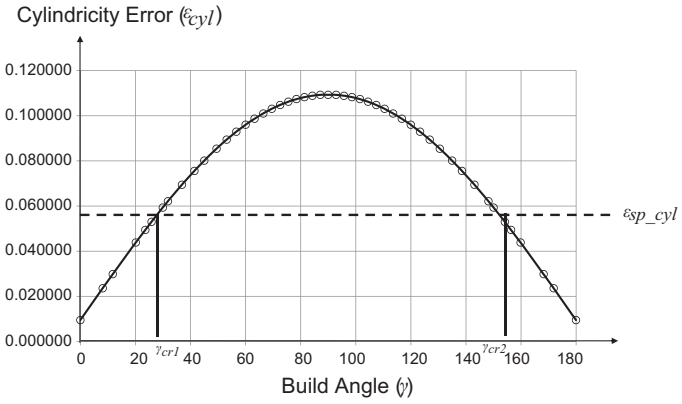

Fig. 2. Critical regions of orientation for cylindricity error in LM [7].

Arni and Gupta [12] found similar critical regions for flatness errors induced in a planar feature in LM. According to their results the flatness error (ε_f) is given as $\varepsilon_f = \Delta z \cdot \cos\gamma$, where Δz is the slice thickness and γ is the angle between the normal to the plane ($\overrightarrow{n_p}$) and the build vector ($\overrightarrow{bv}$). If a flatness callout is specified on a planar feature (ε_{sp_f}) in the part design, then the flatness error induced on that feature will be less than the specified value only if γ lies within the critical regions. The critical regions for flatness errors as described in [12] are shown in Fig. 3.

The feasibility regions for cylindricity and flatness errors described in the above sections have been modified in this paper to develop an algorithm to calculate a combined optimal orientation for minimal cylindricity and flatness form errors. For both the cylindricity and flatness errors, the feasible orientation regions are mapped from the 3D space onto a 1D line space and this line space is then used to develop an optimization model which will calculate the orientation corresponding to minimum form errors in the part features. The algorithm is explained in details in the following sections.

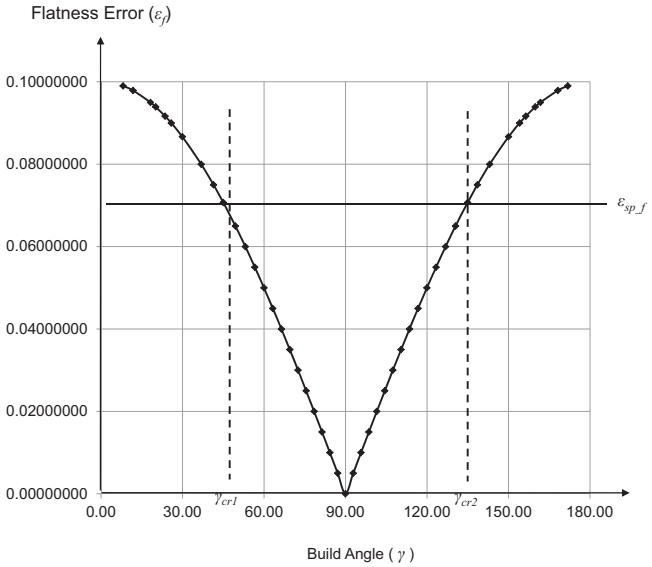

Fig. 3. Critical regions of orientation for flatness error in LM. Adapted from [12].

3.1. Mapping of feasible orientation regions for cylindricity error

Let a part have n_{cyl} critical cylindrical and n_f critical planar features. From the description in the above section, it is known that for the ith cylindrical feature with a certain specified tolerance callout $\varepsilon^i_{sp\_cyl}$, the cylindricity error will lie within the tolerance limits if the angle, γ^i_{cyl}, between the unit cylinder axis of the feature ($\overrightarrow{ca^i}$) and the build vector ($\overrightarrow{bv}$) lies within the tolerance critical regions. Mathematically this can be written as:

$$0 \le \gamma^i_{cyl} \le (\gamma_{cr1})^i_{cyl} \quad \text{and} \quad (\gamma_{cr2})^i_{cyl} \le \gamma^i_{cyl} \le 180$$

where $(\gamma_{cr1})^i_{cyl}$ and $(\gamma_{cr2})^i_{cyl}$ are the lower and upper critical limits of the tolerance feasibility zones of the ith cylindrical feature respectively. However, $(\gamma_{cr2})^i_{cyl} = 180 - (\gamma_{cr1})^i_{cyl}$. Therefore,

$$0 \le \gamma^i_{cyl} \le (\gamma_{cr1})^i_{cyl} \quad \text{and} \quad 180 - (\gamma_{cr1})^i_{cyl} \le \gamma^i_{cyl} \le 180$$

Taking cosines on both sides,

$$\cos((\gamma_{cr1})^i_{cyl}) \le \cos(\gamma^i_{cyl}) \le 1 \quad \text{and} \quad -1 \le \cos(\gamma^i_{cyl}) \le -\cos((\gamma_{cr1})^i_{cyl})$$
$$\Rightarrow (c_{cr})^i_{cyl} \le (c_z)^i_{cyl} \le 1 \quad \text{and} \quad -1 \le (c_z)^i_{cyl} \le -(c_{cr})^i_{cyl} \tag{1}$$

where $c = \cos(\gamma)$ and $(c_z)^i_{cyl}$ is the z-component of $\overrightarrow{ca^i}$. Taking squares on both sides and collecting the terms, Eq. (1) can be written as:

$$\left(c^2_{cr}\right)^i_{cyl} \le \left(c^2_z\right)^i_{cyl} \le 1 \tag{2}$$

In other words, for the cylindricity tolerance to be satisfied, the square of the z-component of $\overrightarrow{ca^i}$ should be between the square of the cosine of the lower critical angle for that cylinder and 1. If the values of the square of the z-component of $\overrightarrow{ca^i}$ are plotted on a line, the feasible and infeasible regions can be depicted as shown in Fig. 4. Therefore, Eq. (2) represents a mapping from a 3D euclidean space of the feasible and infeasible regions for the part orientation to a 1D line space. This reduction of the dimensionality of the error space from 3D to 1D leads to a simplified objective function for minimizing the total errors, as shown in the following sections.

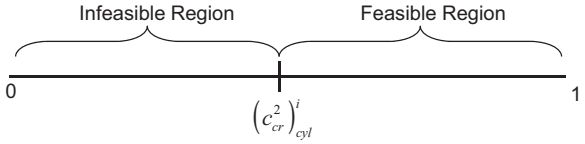

Fig. 4. 1D orientation feasibility regions for cylindricity error.

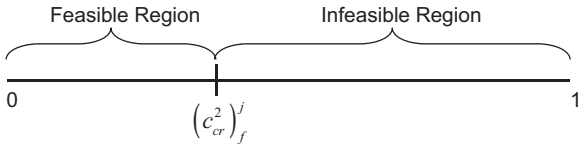

Fig. 5. 1D orientation feasibility regions for flatness error.

3.2. Mapping of feasible orientation regions for flatness error

Similar to the cylindricity error described in the previous section, the feasibility region for flatness error can also be mapped on to a 1D line. The mapping of the flatness form error presented in this section is an extension of the analysis performed on flatness errors in LM processes by Arni and Gupta [12]. From [12] and from Fig. 3, for a flat feature (j), the mathematical relationship can be written as:

$$(\gamma_{cr1})^j_f \le \gamma^j_f \le (\gamma_{cr2})^j_f \Rightarrow (\gamma_{cr1})^j_f \le \gamma^j_f \le 180 - (\gamma_{cr1})^j_f \tag{3}$$

where, γ^j_f is the angle between the build vector ($\overrightarrow{bv}$) and the unit normal ($\overrightarrow{n^j_p}$) to the jth planar feature. $(\gamma_{cr1})^j_f$ and $(\gamma_{cr2})^j_f$ are the lower and upper bounds of the tolerance feasibility region of the jth planar feature. Taking cosines on both sides for Eq. (3):

$$-\cos((\gamma_{cr1})^j_f) \le \cos(\gamma^j_f) \le \cos((\gamma_{cr1})^j_f) \Rightarrow -(c_{cr})^j_f \le (c_z)^j_f \le (c_{cr})^j_f$$

where $c = \cos(\gamma)$ and $(c_z)^i_f$ is the z-component of $\overrightarrow{n^j_p}$. Taking squares on both sides,

$$0 \le \left(c^2_z\right)^j_f \le \left(c^2_{cr}\right)^j_f \tag{4}$$

Therefore, to satisfy flatness tolerance, the square of the z-component of $\overrightarrow{n^j_p}$ should be between 0 and the square of the cosine of the lower critical angle. The feasible regions for satisfying the flatness tolerance of a planar feature can be plotted on a 1D line, similar to the cylindricity tolerance, as shown in Fig. 5, which leads to a more simplified objective function for minimizing the errors.

3.3. Optimal orientation for minimum cylindricity and flatness errors

In this section a multi-objective weighted penalty-based optimization model is developed using the 1D feasible regions for cylindricity and flatness errors. This optimization model calculates the part orientation corresponding to the minimum errors in the part.

For a part with multiple cylindrical and planar features, a potential candidate for the optimal build direction would be one for which the squares of the z-component of each cylindrical axis and each normal to the plane lie within its respective feasible regions. A penalty is imposed on a feature if it deviates away from its individual optimal orientation. The individual optimal orientation corresponds to 1 for cylindrical features and 0 for planar features on the 1D line space (developed in Sections 3.1 and 3.2 respectively). Therefore, for the ith cylinder and the jth planar feature, the

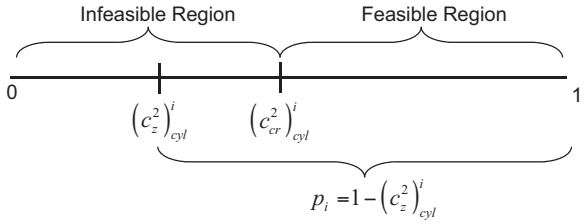

Fig. 6. Penalty for a cylindrical feature.

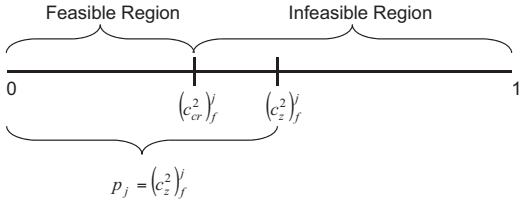

Fig. 7. Penalty for a flat feature.

penalties associated with them are $p_i = 1 - \left(c_z^2\right)_{cyl}^i$ and $p_j = \left(c_z^2\right)_f^j$ respectively, as shown in Figs. 6 and 7.

If ω_i and ω_j are user-defined weights associated with each cylindrical feature and planar feature respectively such that $\sum_{i=1}^{n_{cyl}} \omega_i + \sum_{j=1}^{n_f} \omega_j = 1$, then the error function can be written as $f(\theta, \phi) = \sum_{i=1}^{n_{cyl}} p_i \omega_i + \sum_{j=1}^{n_f} p_j \omega_j$. This error function varies as the part is rotated about the x and y axes by angles θ and ϕ and forms the objective function of a combined optimization model for calculating the optimal orientation for minimum form errors. Mathematically the optimization model can be written as:

$$\begin{aligned} &\text{Min} \quad f(\theta, \phi) = \sum_{i=1}^{n_{cyl}} p_i \omega_i + \sum_{j=1}^{n_f} p_j \omega_j \\ &s.t. \quad \left(c_{cr}^2\right)_{cyl}^i \le \left(c_z^2\right)_{cyl}^i \le 1, i = 1, 2, 3, \ldots, n_{cyl} \\ &0 \le \left(c_z^2\right)_f^j \le \left(c_{cr}^2\right)_f^j, i = 1, 2, 3, \ldots, n_f \\ &0 \le \theta \le 360^\circ \\ &0 \le \phi \le 360^\circ \\ &\sum_{i=1}^{n_{cyl}} \omega_i + \sum_{j=1}^{n_f} \omega_j = 1 \end{aligned} \tag{5}$$

The above optimization model will find the optimal values of θ and ϕ i.e. θ_{opt} and ϕ_{opt} which will lead to minimum cylindricity and flatness errors in the part features. The first constraint of the optimization model ensures that the cylindricity tolerance callouts on all the cylindrical features are satisfied while the second constraint makes sure that all the flatness callouts are satisfied. The weights ω_i and ω_j provide a means to the user to vary the relative importance of each feature depending upon the part design and usage. The above optimization model is used to calculate the optimal orientation for two test parts shown in Figs. 8 and 9.

The first test part has two critical cylindrical bosses (C_1 and C_2) of radii 10 mm and two critical planar surfaces (F_1 and F_2). At the default orientation, the cylinder axis of the boss C_1 is oriented in direction (1, 0, 0) and the cylindricity callout specified on C_1 is 0.096 mm. The other boss, C_2 is oriented in the

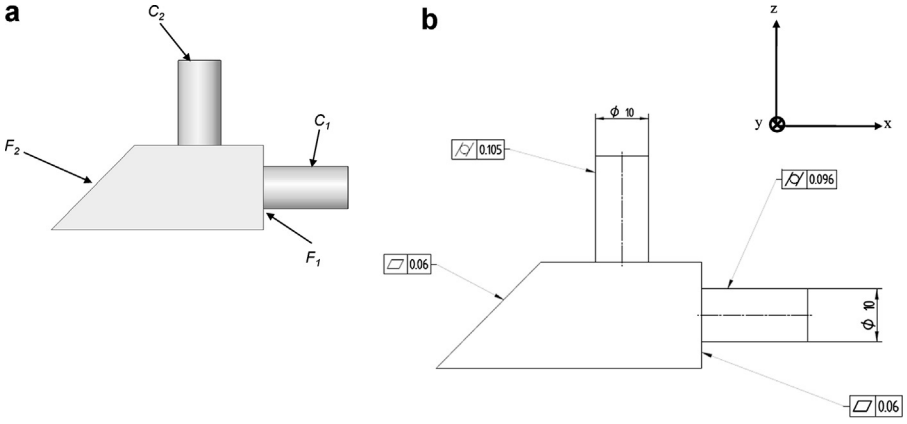

Fig. 8. (a) Test Part 1 and (b) tolerance callouts on Test Part 1.

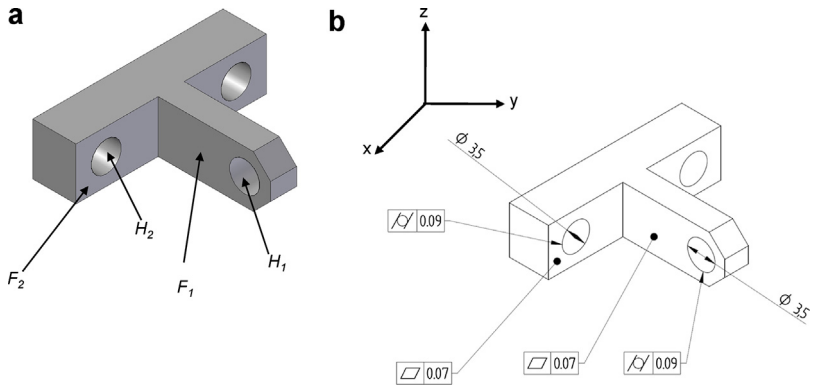

Fig. 9. (a) Test Part 2 and (b) tolerance callouts on Test Part 2.

Table 1
Optimization results for Test Part 1 for minimum error.

Feature	C_1	C_2	F_1	F_2
Form tolerance callout (mm)	0.096	0.105	0.060	0.060
Form error at original orientation (mm)	0.110	0.000	0.000	0.071
Form error at optimal orientation (mm)	0.0866	0.050	0.050	0.0259
Original orientation (c_x, c_y, c_z)	1.00, 0.00, 0.00	0.00, 0.00, 1.00	1.00, 0.00, 0.00	−0.71, 0.00, 0.71
Optimal orientation (c_x, c_y, c_z)	0.43, 0.75, −0.50	−0.25, −0.43, −0.86	0.43, 0.75, −0.50	−0.48, −0.84, −0.26

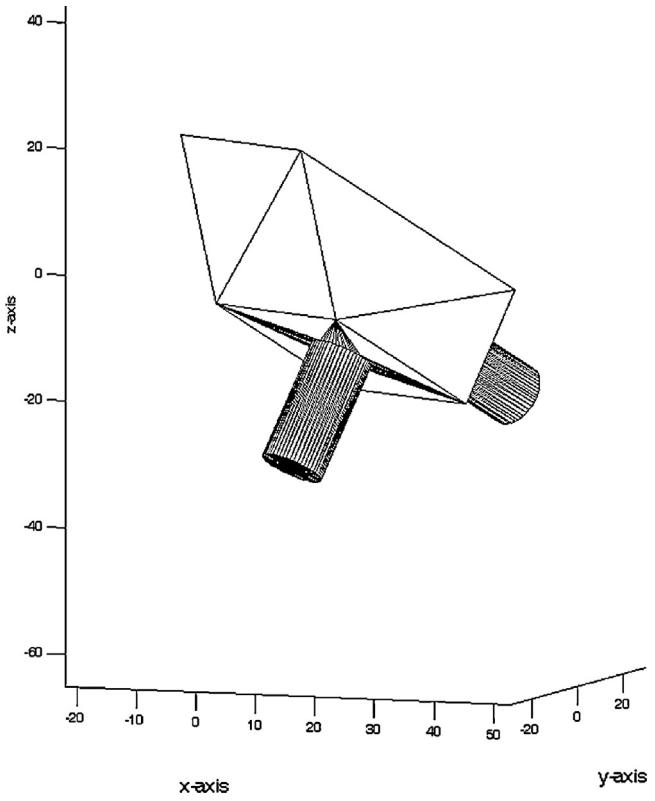

Fig. 10. Optimal orientation for Test Part 1 for minimum error.

direction (0, 0, 1) and has a cylindricity tolerance callout of 0.105 mm. Both the planar surfaces have flatness callouts of 0.06 mm; the first flat feature (F_1) has its unit normal oriented in the direction (1, 0, 0) while the second flat feature (F_2) is oriented in the direction (−0.7071, 0, 0.7071). If the part is built in this orientation the callout on the features F_1 and C_2 are satisfied but those of C_1 and F_2 are not, as shown in Table 1. The optimal orientation for the part is found using the optimization model presented in Eq. (5) with equal weights of 0.25 assigned to each of the four features. This optimization model is solved using the non-linear constrained optimization routine, fmincon, provided in the MATLAB package [33]. In this paper, the trust-region-reflective algorithm has been selected in the fmincon program for solving the optimization problem. This routine is also used for solving the other optimization models that have been presented in the following sections of the paper. The weights are chosen arbitrarily in this case but the user can choose the weights according to his/her preferences. According to the optimization results, the part has to be rotated by angles $\theta_{opt} = 178.67$ and $\phi_{opt} = 30$ degrees about the x- and y-axes to obtain the optimal orientation, as shown in Fig. 10. In this orientation all the tolerance callouts are satisfied. The consolidated results are shown in Table 1.

Similar to Test Part 1, the optimization model given in Eq. (5) is used to calculate the optimal part orientation for the Test Part 2. Test Part 2 has two critical cylindrical holes H_1 and H_2 each having a cylindricity tolerance callout of 0.09 mm; H_1 is oriented

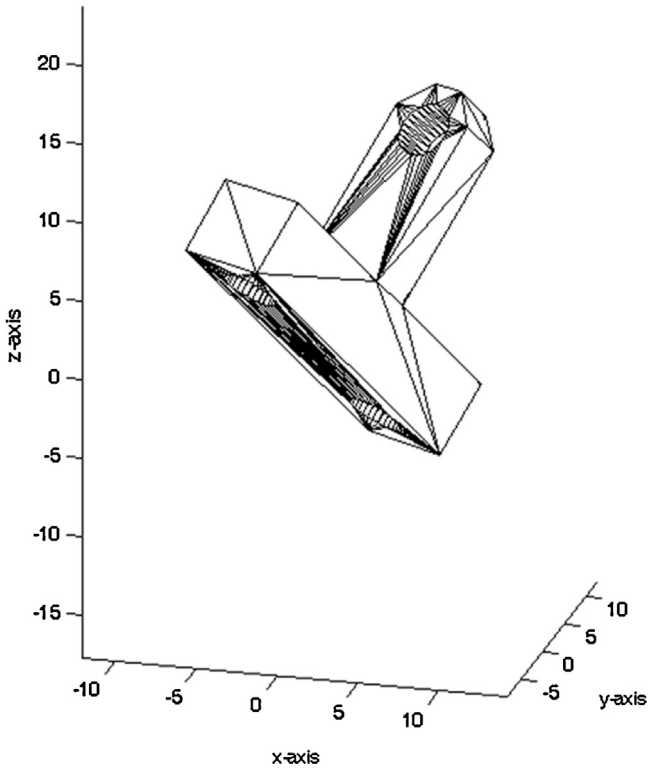

Fig. 11. Optimal orientation for Test Part 2 for minimum error.

in the direction (−1,0,0) and H_2 is oriented in the direction (0,1,0). The planar surfaces F_1 and F_2 have a callout of 0.07 mm and their normals are oriented in the directions (−1, 0, 0) and (0, 1, 0) respectively. Weights of 0.3 are assigned to each of the cylinders while weights of 0.2 are assigned to each of the planes, thereby giving more importance to the cylindrical features. Similar to Test Part 1, the weights are chosen based on user preference. According to the results of the optimization algorithm, the part has to be rotated by $\theta_{opt} = 89.6$ and $\phi_{opt} = 45$ degrees about the x- and y-axes to obtain the optimal orientation and is shown in Fig. 11. The consolidated results are provided in Table 2.

Thus, the optimization algorithm is able to find an orientation which results in minimum form error for all the features. However, there are generally several candidate local optimal build directions which will minimize the desired errors. Since Eq. (5) is a non-linear optimization, depending upon the starting orientation, any of the candidate build directions can be reached. But among these multiple candidate optimal orientations, some of them will invariably lead to higher amount of support structures as compared to others. Since support structures are considered to be process waste, it is desirable to calculate an optimal direction that minimizes support structures while achieving the required tolerances. However, the calculation of the volume of support structures is not straightforward, particularly if the part is non-convex. Therefore, a new voxel-based approach has been developed to calculate the volume of support structures (V_S). The approach is explained in detail in the following section.

Table 2
Optimization results for Test Part 2 for minimum error.

Feature	H_1	H_2	F_1	F_2
Form tolerance callout (mm)	0.090	0.090	0.070	0.070
Form error at original orientation (mm)	0.110	0.110	0.000	0.000
Form error at optimal orientation (mm)	0.0707	0.0707	0.0707	0.0707
Original orientation (c_x, c_y, c_z)	−1.00, 0.00, 0.00	0.00, 1.00, 0.00	−1.00, 0.00, 0.00	0.00, 1.00, 0.00
Optimal orientation (c_x, c_y, c_z)	−0.35, −0.61, 0.71	0.35, 0.62, 0.71	−0.35, −0.61, 0.71	0.35, 0.62, 0.71

4. Calculation of support structure volume

Support structures are used in the production of LM parts whenever there are internal cavities or overhanging features [1]. This section describes a voxel-based algorithm for calculating the volume of support structures that is required for a part built in LM. Voxels are cubes of equal sizes which are used to decompose the volume of the CAD part [20–23]. In the current algorithm, the Stereolithography (STL) file of the part is converted to a voxel representation by the methodology presented in [20] using the MATLAB implementation developed by [34]. The STL file is the standard input file for all RP/LM machines and approximates the part surface with triangular facets. In the voxel representation of the STL file, each cube is either filled with material or completely empty. Once the voxel cubes are generated, the trapped empty voxels are calculated for each column of voxels in the part representation to obtain the location and total volume of support structures. These trapped empty voxels are referred to as support voxels and they represent the spaces within the part volume which will require support structures.

The voxel representation as shown Fig. 12 obtained from the STL file consists of two types of voxels: filled and unfilled. Filled voxels make up the part volume while unfilled voxels are the empty spaces in 3D space. Values of 1 are assigned to the filled voxels and 0 to the unfilled voxels as shown in Fig. 13.

The algorithm for calculating the support structures from voxels is explained in this section with a 2D part for the sake of simplicity and can be extended to a 3D part. The voxelized model obtained from the STL file also contains the bounding box of the part, as shown in Fig. 13. Starting from the top left rear corner (assuming a right hand coordinate system) on the top of the bounding box, the voxels are counted downwards along the column toward the base for the first voxel column and the number of support voxels is

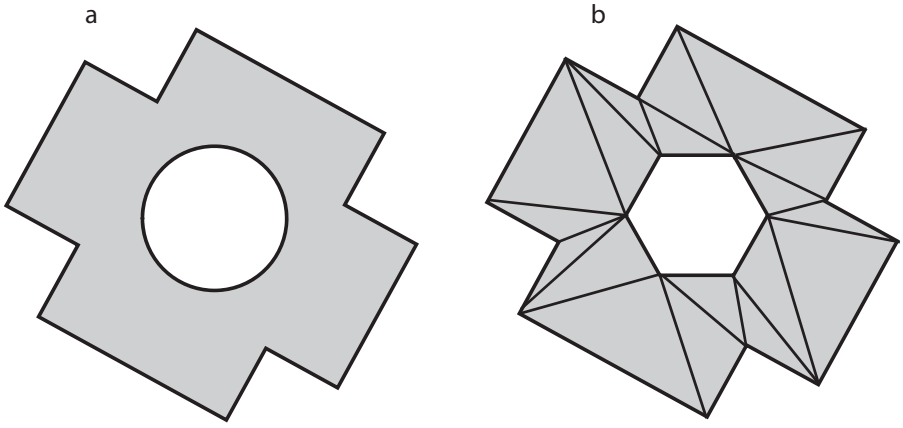

Fig. 12. (a) Part and (b) STL file.

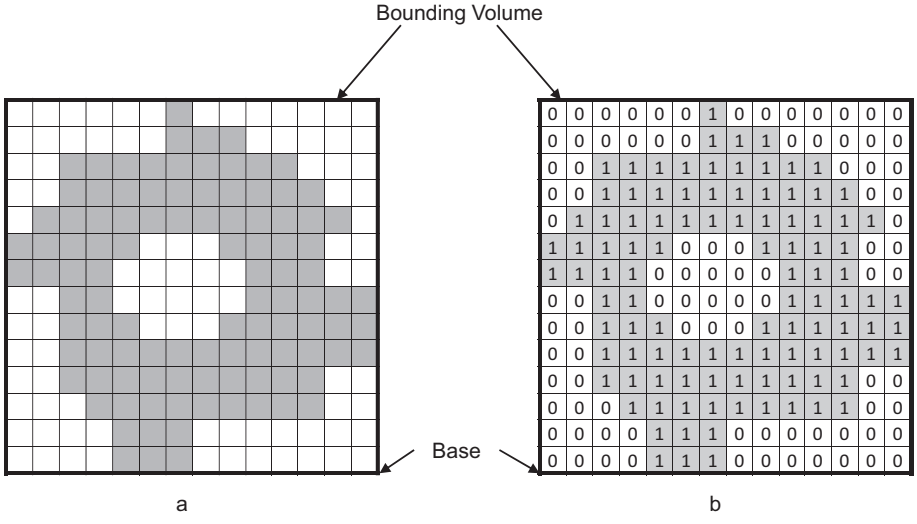

Fig. 13. (a) Voxelized representation of the part and (b) Voxel cell values.

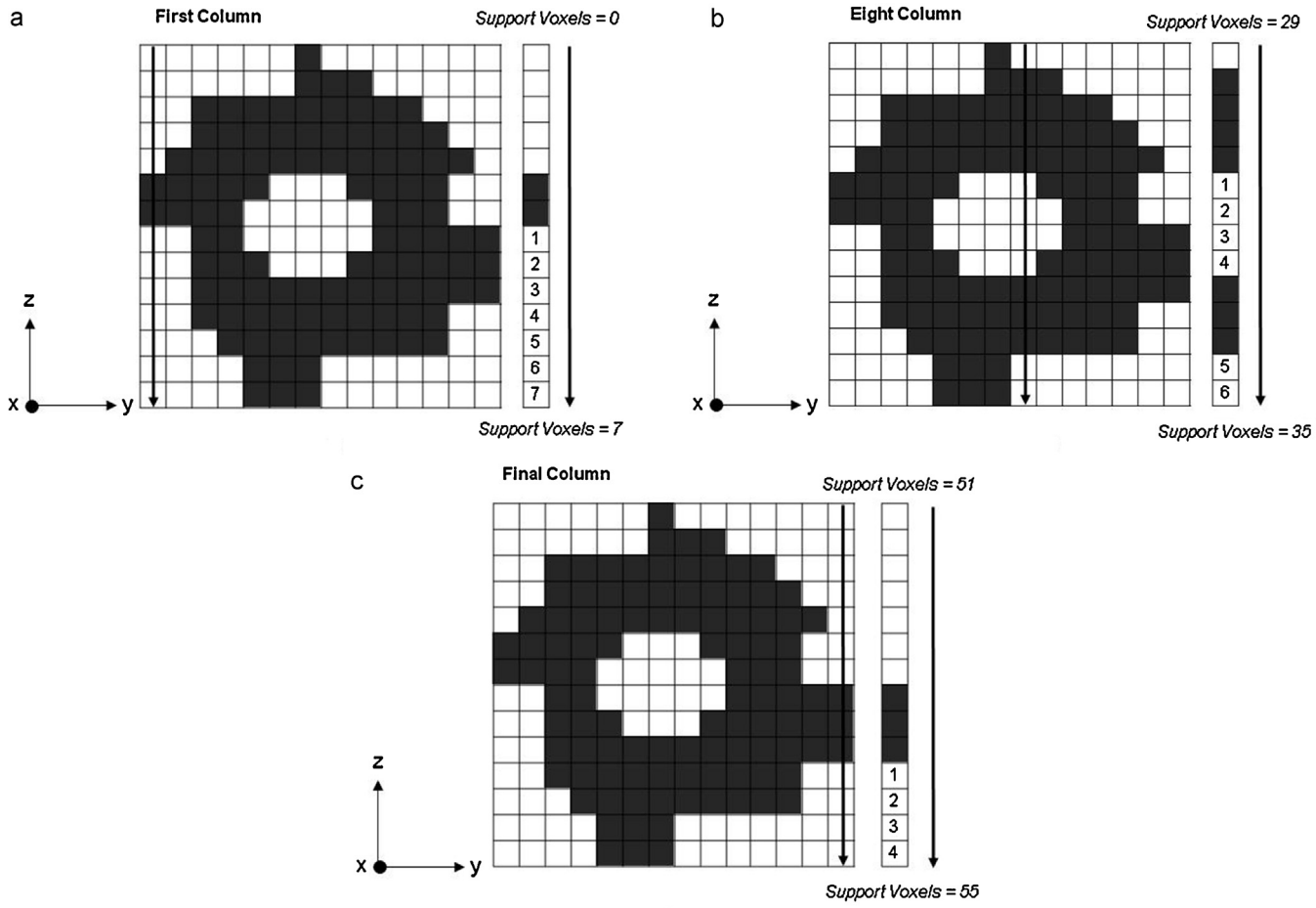

Fig. 14. (a) First pass, (b) second pass and (c) final pass for the algorithm to calculate support structures.

calculated for that column. An empty voxel is classified as a support voxel if it satisfies any of the following criteria:

(i) It is a member of a contiguous array of empty voxels that is bounded on both sides i.e. between top and bottom, by full voxels.
(ii) It is a member of a contiguous array of empty voxels that is bounded on the top by a full voxel and on the bottom by the base.

At the start of the first array, the total number of support voxels is taken as zero. After the first column has been scanned, the total number of support voxels is incremented by the number of support voxels present in the first column. All the columns in the bounding box are scanned similarly and the total number of support voxels at the end of the final array provides the total number of support voxels, N_S, for the part. The number of support voxels multiplied by the volume of a voxel provides the volume of support structures for the part. Fig. 14a shows the first pass of the algorithm where the support voxels for the first column are calculated while Fig. 14b and c shows the calculation for the eighth and final column respectively. In Fig. 14, the numbered empty voxels on the right most column represent the support voxels for each column. Fig. 15 shows the support structures (in black) for the part. The algorithm is applied on two test parts to calculate the support structures and the results are shown in Figs. 16 and 17.

5. Part orientation for minimal support structure volume

In the previous section, a voxel-based algorithm to calculate the volume of support structures for a part built in LM was introduced. In this section, this algorithm will be applied to calculate the optimal part orientation for minimum support structure volume.

An optimization model is developed with the volume of support structures, V_S as the objective problem which is a function of θ and

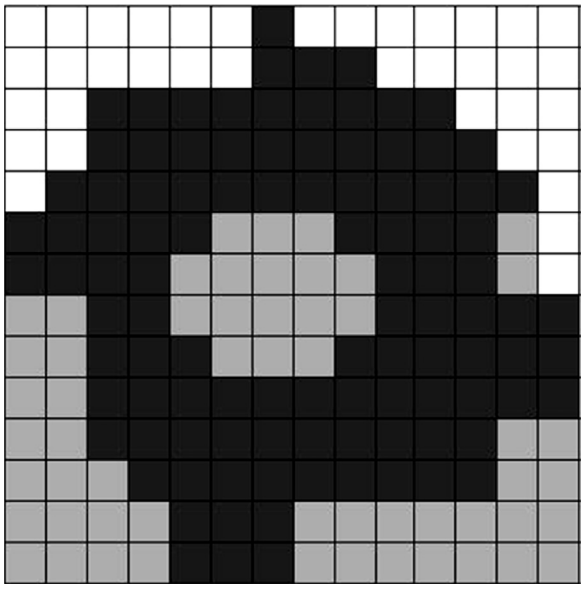

Fig. 15. Support structures, in gray color.

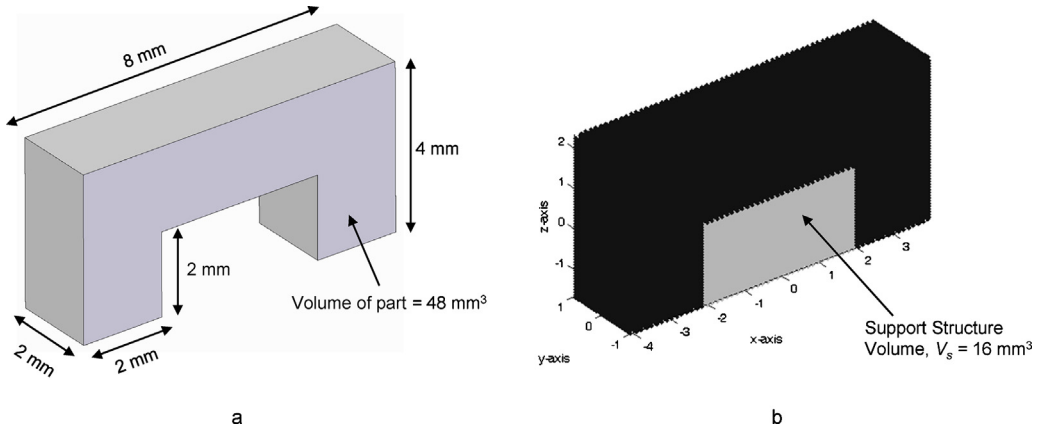

Fig. 16. (a) Part and (b) support structures, shown in light gray.

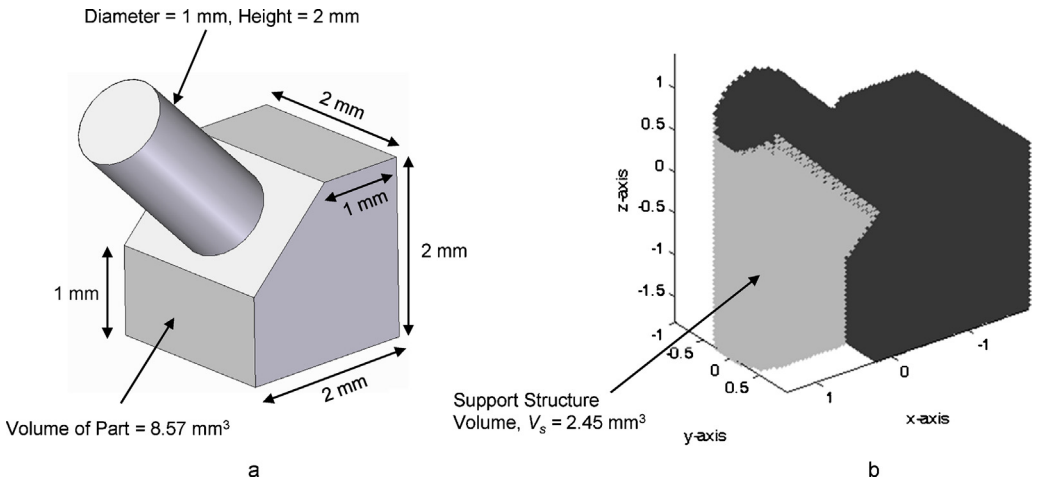

Fig. 17. (a) Part and (b) support structures, shown in light gray.

ϕ. θ and ϕ are the angles by which the part is rotated about the x- and y-axes to find the optimal support structure volume (V_{S_opt}). The errors specified on the cylindrical and planar features on the part are used as constraints in the optimization model similar to Eq. (3). Mathematically the optimization model can be written as:

$$\begin{aligned} &\text{Min} \quad f(\theta, \phi) = V_S \\ &s.t. \left(c_{cr}^2\right)_{cyl}^{i} \le \left(c_z^2\right)_{cyl}^{i} \le 1, i = 1, 2, 3, \ldots, n_{cyl} \\ &0 \le \left(c_z^2\right)_f^j \le \left(c_{cr}^2\right)_f^j, i = 1, 2, 3, \ldots, n_f \\ &0 \le \theta \le 360^\circ \\ &0 \le \phi \le 360^\circ \end{aligned} \tag{6}$$

Eq. (6) is used to find the optimal part build for minimum support structure for the two test parts, shown in Figs. 8 and 9 while satisfying the flatness and cylindricity callouts. Using the optimization model on Test Part 1, the optimal values of θ and ϕ are calculated as $\theta_{opt} = 121.40$ and $\phi_{opt} = 33.65$ degrees. The optimal orientation of the test part along with the support structures (light gray) is shown in Fig. 18. In this optimal orientation the tolerances for all the critical features will be satisfied due to the form error constraints in the optimization model. The results are presented in Table 3. The support structures required in this orientation is **28.91%** less than that the support structures required in the orientation for minimum error, shown in Table 5.

Similarly, the optimal orientation for minimum support structure for Test Part 2 is calculated and according to the optimization results, the part has to be rotated by $\theta_{opt} = 54.24$ and $\phi_{opt} = 37.66$ degrees about the x- and y-axes to find the optimal orientation. Fig. 19 shows the optimal orientation of the part along with the support structures while Table 4 shows the errors for each of the features at this optimal orientation. Table 5 shows that at this orientation there is a **35.02%** reduction in the volume of support structures when compared to the orientation for minimum error.

In this section an algorithm to find the optimal orientation based on minimum support structures was developed and tested on two sample parts. This algorithm will provide practitioners a simple

Table 3
Optimal orientation for minimum V_S for Test Part 1.

Feature	C_1	C_2	F_1	F_2
Form tolerance callout (mm)	0.096	0.105	0.060	0.060
Form error at optimal orientation (mm)	0.084	0.095	0.055	0.008
Optimal orientation (c_x, c_y, c_z)	0.26, 0.79, −0.55	0.72, −0.54, −0.43	0.26, 0.79, −0.55	0.33, −0.94, 0.08
Volume of support structures, V_S (mm³)	19,993.03			

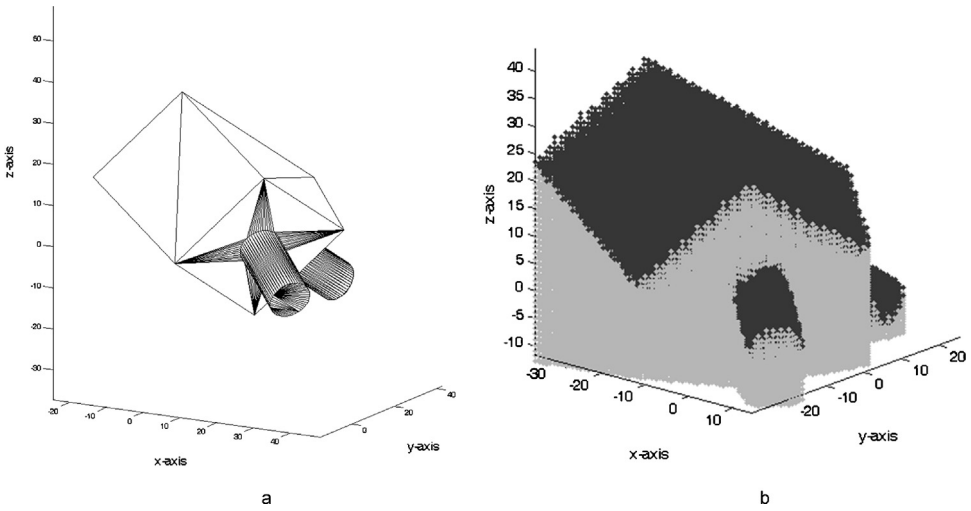

Fig. 18. (a) Test Part 1 optimal orientation for minimum support structures and (b) support structures (gray) at optimal orientation.

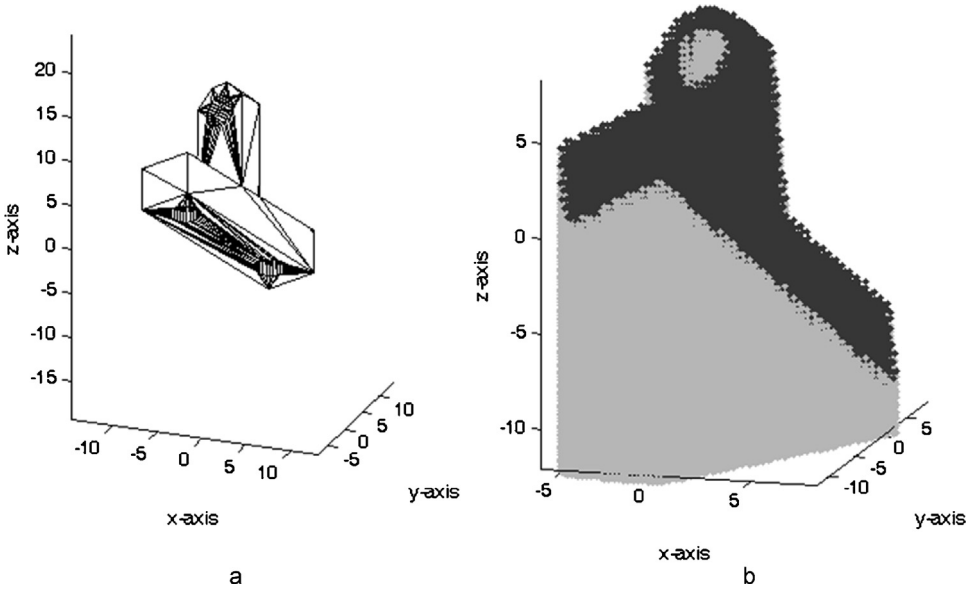

Fig. 19. (a) Test Part 2 optimal orientation for minimum support structures and (b) support structures (gray) at optimal orientation.

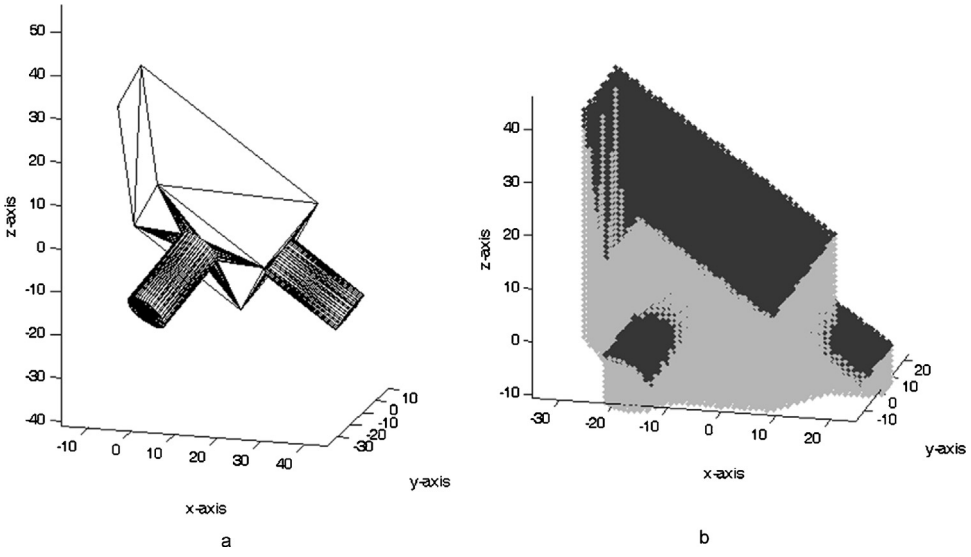

Fig. 20. (a)Test Part 1 optimal orientation for minimum error and minimum support structures and (b) support structures (gray) at optimal orientation.

Table 4
Optimal orientation for minimum V_S for Test Part 2.

Feature	H_1	H_2	F_1	F_2
Form tolerance callout (mm)	0.090	0.090	0.070	0.070
Form error at optimal orientation (mm)	0.080	0.078	0.061	0.064
Optimal orientation (c_x, c_y, c_z)	0.38, −0.69, 0.61	−0.27, 0.72, 0.64	0.38, −0.69, 0.61	−0.27, 0.72, 0.64
Volume of support structures, V_S (mm^3)	1379.49			

Table 5
Comparison between support structures between optimal orientation for minimum error only and orientation for minimum support structure.

	Orientation for min. form error only	Orientation for min. support structure while satisfying tolerance callouts	% Reduction
V_{S_opt} Test Part 1 (mm^3)	28,124.37	19,993.03	28.91
V_{S_opt} Test Part 2 (mm^3)	2123.00	1379.49	35.02

unified procedure to determine the best orientation to minimize the support structures while satisfying the tolerance callouts on the part.

6. Part orientation for minimum form errors and support structure volume

In the previous section, an objective function was developed to calculate a build direction to minimize the support structures while achieving the required tolerances. Sometimes the application may demand that both the part errors and support structures be minimized simultaneously. However, these two parameters are not directly proportional to each other. A particular orientation may lead to lesser errors but it may not necessarily reduce the support structures and vice versa. Thus an algorithm must be designed such that these two conflicting parameters are minimized together. In this section a multi-objective optimization model is developed which seeks to achieve this objective by minimizing cylindricity and flatness form errors in a part along with the volume of support structures by varying the part orientation.

A single weighted aggregate optimization function (AOF) has been constructed with the form error function developed in Section 3.3 and the volume of support structures, V_S, developed in Section 4. However the error is in the range of 0–1 while the support structures are not confined to this range. Therefore, the support structure volume is normalized to the range of 0–1 according to the following equation:

$$V_{S\_norm}(\theta, \phi) = \frac{V_S(\theta, \phi) - V_{S\_min}}{V_{S\_max} - V_{S\_min}} \tag{7}$$

where $V_S(\theta, \phi)$ is the support structure at any θ and ϕ, V_{S_min} and V_{S_max} are the minimum and maximum support structure volumes among all the possible particular combinations of θ and ϕ. The values of V_{S_min} and V_{S_max} in Eq. (7) can be calculated by the optimization model given in Eq. (6) by removing the constraints. Using $V_{S\_norm}(\theta, \phi)$, the weighted AOF can be written as: $\sum_{i=1}^{n_{cyl}} p_i\omega_i + \sum_{j=1}^{n_f} p_j\omega_j + \omega_S V_{S\_norm}$, where ω_i is the weight for the ith cylinder, ω_j is the weight for the jth planar feature and ω_S is the weight for the normalized support structure volume. The weights are selected such that $\sum_{i=1}^{n_{cyl}} \omega_i + \sum_{j=1}^{n_f} \omega_j + \omega_S = 1$, n_{cyl} = number of cylindrical features and n_f = number of flat features in the part. The multi-objective optimization model can be written as:

$$\begin{aligned}
&f(\theta, \phi) = \sum_{i=1}^{n_{cyl}} p_i\omega_i + \sum_{j=1}^{n_f} p_j\omega_j + \omega_S V_{S_norm} \\
&s.t. \left(c_{cr}^2\right)_{cyl}^{i} \le \left(c_z^2\right)_{cyl}^{i} \le 1, i = 1, 2, 3, \ldots, n_{cyl} \\
&0 \le \left(c_z^2\right)_f^j \le \left(c_{cr}^2\right)_f^j, i = 1, 2, 3, \ldots, n_f \\
&0 \le \theta \le 360^\circ \\
&0 \le \phi \le 360^\circ \\
&\sum_{i=1}^{n_{cyl}} \omega_i + \sum_{j=1}^{n_f} \omega_j + \omega_S = 1
\end{aligned} \tag{8}$$

The multi-objective optimization model given in Eq. (8) is used to find the optimal part orientation for minimum form error and minimum support structure volume for the two test parts shown in Figs. 8 and 9. The constraints ensure that the critical part features are within their specified tolerance callouts. For Test Part 1, weights for the cylindrical features are chosen as 0.2 each, for the planar features as 0.15 each and for the support structures as 0.3.

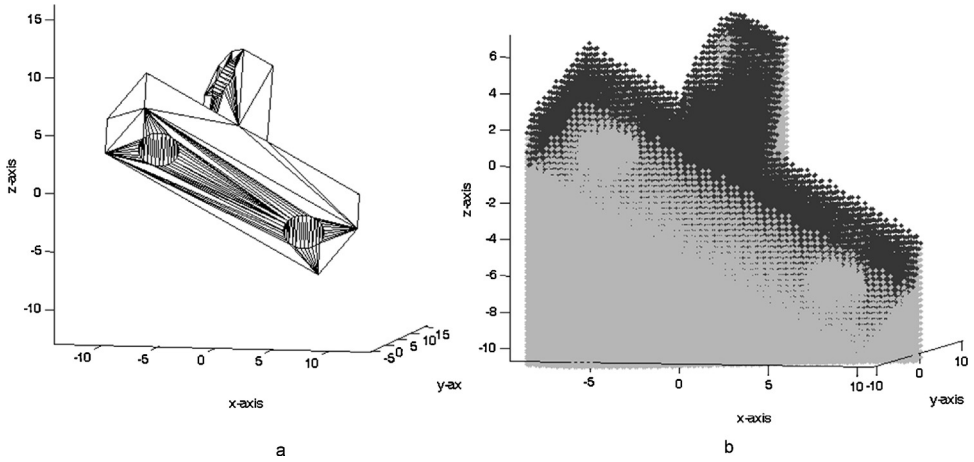

Fig. 21. (a) Test Part 2 optimal orientation for minimum error and minimum support structures and (b) support structures (gray) at optimal orientation.

Table 6
Optimal orientation for minimum error and minimum V_S for Test Part 1.

Feature	C_1	C_2	F_1	F_2
Form tolerance callout (mm)	0.096	0.105	0.060	0.060
Form error at optimal orientation (mm)	0.087	0.080	0.050	0.001
Optimal orientation (c_x, c_y, c_z)	0.61, 0.61, −0.50	−0.42, −0.68, −0.60	0.61, 0.61, −0.50	−0.88, −0.48, −0.01
Volume of support structures, V_S (mm^3)	25,100.95			

Table 7
Optimal orientation for minimum error and minimum V_S for Test Part 2.

Feature	H_1	H_2	F_1	F_2
Form tolerance callout (mm)	0.090	0.090	0.070	0.070
Form error at optimal orientation (mm)	0.087	0.087	0.050	0.050
Optimal orientation (c_x, c_y, c_z)	−0.75, −0.43, 0.50	−0.16, 0.85, 0.50	−0.75, −0.43, 0.50	−0.16, 0.85, 0.50
Volume of support structures, V_S (mm^3)	1541.87			

Table 8
Comparison between support structures between optimal orientation for minimum error and orientation for minimum error and support structures.

	Orientation for min. error	Orientation for min. error and min. support structures	% Reduction
V_{S_opt} Test Part 1 (mm^3)	28,124.37	25,100.95	10.75
V_{S_opt} Test Part 2 (mm^3)	2078.56	1541.87	25.82

For Test Part 2, weights for the cylinder, the planar features and the support structures are all set equally to 0.2. According to the optimization results, the values of θ_{opt} and ϕ_{opt} for Test Part 1 are 137 and 35.28 degrees respectively and for Test Part 2 are 35.5 and 30 degrees respectively. The optimal orientations along with the support structures for Test Part 1 and Test Part 2 are shown in Figs. 20 and 21. The optimization results for the parts are shown in Tables 6 and 7. Table 8 shows that there is a **10.75%** reduction in support structures for Test Part 1 and **25.82%** for Test Part 2 for this orientation as compared to the optimal orientation for minimum error alone.

Thus the multi-objective optimization model presented in section was able to minimize both the cylindricity and flatness form errors and the volume of support structures simultaneously for a part built in LM by calculating the optimal part orientation.

7. Conclusions and future scope

The focus of this paper was to analyze the manufacturing of precision parts through LM processes with minimal amount of support structures by selecting the optimal part orientation. Manufacturing of precision parts require near zero levels of part errors and in this paper, a combined error function was developed for LM processes which correlated cylindricity and flatness errors with part orientation and calculated the part orientation for minimum errors. One of the main contributors to the energy and material consumption in LM processes are the support structures that are used to hold up overhangs and internal cavities. A voxel-based algorithm was developed to calculate the volume of support structures for a particular part orientation. The voxel algorithm was applied to find the optimal part orientation for minimum support structure volume and reductions of around **29–35%** were achieved as compared to orientation for minimum error only. The minimization of support structures was achieved while still satisfying the tolerance callouts on critical features. The error function and the support structure volume function were then combined together to generate a single aggregate function. This aggregate function, when used in an optimization model, provides the engineer a single solution for the optimal part orientation for minimal error and support structures. The combined optimization was able to reduce the volume of support structures by almost **11–26%** for the two test cases as compared to the orientation for minimum error only. The algorithm also offers the user with option of choosing appropriate weights for each tolerance callout and the total volume of support structures. This provides a means to tailor the algorithm based on individual preferences and emphasis on different tolerance callouts and extent of support structures. Thus, the combined methodology presents the LM practitioner a means to manufacture high precision parts with minimal errors while simultaneously minimizing the raw material consumption by reducing the volume of support structures.

The production of error free high precision parts with minimal material utilization will push LM from a niche to a more widespread industry accepted manufacturing process. However, there are certain aspects of LM processes that need to be researched in details. In this paper, only flatness and cylindricity errors have been minimized. The methodology has to be extended to other GD&T errors such as profile, location, orientation and runout errors. One of the areas that has to be looked into is the correlation between the 2D toolpath and the part errors. The effect of process parameters such as powder size, liquid temperature, laser power, etc. on part errors and process energy should also be analyzed. Another area of interest is the minimization of errors and process energy with respect to the quality of input STL file used in the LM machines. Also, those surfaces which need supports have generally poor surface roughness. Therefore, the sum of areas of faces which need supports also need to be minimized in addition to volume of supports. The current algorithm can be extended to include the area of supports as a minimization criterion.

References

[1] Kulkarni P, Marsan A, Dutta D. A review of process planning techniques in layered manufacturing. Rapid Prototyp J 2000;6(1):18–35.
[2] Sabourin E, Houser SA, Bohn JH. Adaptive slicing using stepwise uniform refinement. Rapid Prototyp J 1996;2(4):20–6.
[3] Starly B, Lau A, Sun W, Lau W, Bradbury T. Direct slicing of STEP based NURBS models for layered manufacturing. Comput-Aided Des 2005;37(4):387–97.
[4] Ma WY, But WC, He PR. NURBS-based adaptive slicing for efficient rapid prototyping. Comput-Aided Des 2004;36(13):1309–25.
[5] Koc B. Adaptive layer approximation of free-form models using marching point surface error calculation for rapid prototyping. Rapid Prototyp J 2004;10(5):270–80.
[6] Hope RL, Roth RN, Jacobs PA. Adaptive slicing with sloping layer surfaces. Rapid Prototyp J 1997;3(3):89–98.
[7] Paul R, Anand S. Optimal part orientation in rapid manufacturing process for achieving geometric tolerances. J Manuf Syst 2011;30(October (4)):214–22.
[8] Thompson DC, Crawford RH. Computational quality measures for evaluation of part orientation in freeform fabrication. J Manuf Syst 1997;16(4):273–89.

[9] Masood SH, Rattanawong W. A generic part orientation system based on volumetric error in rapid prototyping. Int J Adv Manuf Technol 2002;19(3):209–16.
[10] Rattanawong W, Masood SH, Iovenitti P. A volumetric approach to part-build orientations in rapid prototyping. J Mater Process Technol 2001;119(December (1–3)):348–53.
[11] Mankame A, Datseris P, Jouaneh M. Classification and methodologies for orientation and stacking of parts based on internal features. J Manuf Syst 1998;17(6):455–75.
[12] Arni R, Gupta SK. Manufacturability analysis of flatness tolerances in solid freeform fabrication. J Mech Des 2001;123(March (1)):148–56.
[13] Dollar AM, Wagner CR, Howe RD. Embedded Sensors for Biomimetic Robotics Via Shape Deposition Manufacturing; 2006. PT: B; CT: 1st IEEE RAS-EMBS international conference on biomedical robotics and biomechatronics (BioRob 2006); CY: February 20–22, 2006; CL: Pisa, Italy; SP: IEEE; RAS; EMBS; Scuola Superiore Sant Anna; Int Soc Gerontechnol; SIRI; AURION; ONDI; ERA Endoscopy; KTeam; ROBOTECH srl; Carismi; TC: 0; UT: WOS: 000244445100008.
[14] Fadel GM, Kirschman C. Accuracy issues in CAD to RP translations. Rapid Prototyp J 1996;2(2):4–15.
[15] Jamieson R, Hacker H. Direct slicing of CAD models for rapid prototyping. Rapid Prototyp J 1995;1(2):4–12.
[16] Pandey PM, Reddy NV, Dhande SG. Slicing procedures in layered manufacturing: a review. Rapid Prototyp J 2003;9(5):274–88.
[17] Zhou MY, Xi JT, Yan JQ. Adaptive direct slicing with non-uniform cusp heights for rapid prototyping. Int J Adv Manuf Technol 2004;23(1–2):20–7.
[18] Hanumaiah N, Ravi B. Rapid tooling form accuracy estimation using region elimination adaptive search based sampling technique. Rapid Prototyp J 2007;13(3):182–90.
[19] Ollison T, Berisso K. Three-dimensional printing build variables that impact cylindricity. J Ind Technol 2010;26(1):2–10.
[20] Subburaj K, Patil S, Ravi B. Voxel-based thickness analysis of intricate objects. Int J CAD/CAM 2006;6:105–15.
[21] Strasser W, Klein R, Rau R. Geometric modeling: theory and practice: the state of the art. Berlin/New York: Springer; 1997.
[22] Watkins KE, Paus T, Lerch JP, Zijdenbos A, Collins DL, Neelin P, et al. Structural asymmetries in the human brain: a voxel-based statistical analysis of 142 MRI scans. Cereb Cortex 2001;11(9):868–77.
[23] Weese J, Penney GP, Desmedt P, Buzug TM, Hill DL, Hawkes DJ. Voxel-based 2-D/3-D registration of fluoroscopy images and CT scans for image-guided surgery. IEEE Trans Inf Technol Biomed 1997;1(4):284–93.
[24] Allen S, Dutta D. Determination and evaluation of support structures in layered manufacturing. J Des Manuf 1995;5:153–62.
[25] Allen S, Dutta D. On the computation of part orientation using support structures in layered manufacturing. Solid Freeform Fabr Symp 1994;1994:259–69.
[26] Allen S, Dutta D. Wall thickness control in layered manufacturing for surfaces with closed slices. Comput Geom – Theory Appl 1998 JUL;10(4):223–38.
[27] Majhi J, Janardan R, Smid M, Gupta P. On some geometric optimization problems in layered manufacturing. Comput Geom – Theory Appl 1999;12(3–4):219–39.
[28] Majhi J, Janardan R, Smid M, Gupta P. On some geometric optimization problems in layered manufacturing. Algorithms Data Struct 1997;1272:136–49.
[29] Lynn-Charney C, Rosen DW. Usage of accuracy models in stereolithography process planning. Rapid Prototyp J 2000;6(2):77–86.
[30] Liu W, Li L, Kochhar AK. A method for assessing geometrical errors in layered manufacturing. Part 1: error interaction and transfer mechanisms. Int J Adv Manuf Technol 1998;14(9):637–43.
[31] Alexander P, Dutta D. Layered manufacturing of surfaces with open contours using localized wall thickening. Comput-Aided Des 2000;32(March (3)):175–89.
[32] Yang Y, Fuh JYH, Loh HT, Wong YS. Multi-orientational deposition to minimize support in the layered manufacturing process. J Manuf Syst 2003;22(2):116–29.
[33] Constrained Nonlinear Multivariable Optimization Function, http://www.mathworks.com/help/toolbox/optim/ug/fmincon.html [Internet]; c2011 [cited 2011]. Available from: http://www.mathworks.com/help/toolbox/optim/ug/fmincon.html
[34] Mesh Voxelisation Code for MATLAB, The Mathworks. http://www.mathworks.com/matlabcentral/fileexchange/27390-mesh-voxelisation [Internet]; c2010.